Eur. Phys. J. B **48**, 495–500 (2005)
DOI: 10.1140/epjb/e2006-00003-7

THE EUROPEAN PHYSICAL JOURNAL B

Thermal hysteresis of a simulated Al_2O_3 system

V.V. Hoang[a]

Dept. of Physics, College of Natural Sciences, HochiMinh City National University 227 Nguyen Van Cu Str., Distr. 5, HochiMinh City, Vietnam

Received 7 March 2005 / Received in final form 14 August 2005
Published online 19 January 2006 –

Abstract. Thermal hysteresis in a simulated Al_2O_3 system has been investigated using a Molecular Dynamics (MD) method. Simulations were done in the basic cube under periodic boundary conditions containing 3000 ions with Born-Mayer type pair potentials. The system was cooled down from 7000 K to 0 K and heated up from 0 K to 7000 K by the same cooling/heating rate of 1.7178×10^{14} K/s. The temperature dependence of the system density upon cooling and heating shows thermal hysteresis. The differences between structure and dynamics of the models obtained by cooling (MOBC) and heating (MOBH) at three different temperatures of 2100 K, 3500 K and 5600 K have been detected. Calculations show that the differences in the dynamics of the systems are more pronounced than those in the structure. Furthermore, dynamical heterogeneities in MOBC and MOBH at the temperature of 2100 K have been studied through a non-Gaussian parameter and comparison of partial radial distribution functions (PRDFs) for the 10% most mobile or immobile particles with their corresponding mean ones. Cluster size distributions of the 10% most mobile or immobile particles in MOBC and MOBH at the temperature of 2100 K have been obtained. Calculations show that differences in dynamical heterogeneities are pronounced.

PACS. 61.43.Fs Glasses – 78.55.Qr Amorphous materials; glasses and other disordered solids – 61.43.Bn Structural modeling: serial-addition models, computer simulation

1 Introduction

One of characteristic properties of glasses is thermal hysteresis [1]. Jonsson and Andersen investigated icosahedral ordering in Lennard-Jones liquids and glasses upon cooling by MD simulation [1]. They found that at high temperatures the inherent structure was independent of temperature, but slightly above the glass transition temperature T_g the structure changed and local fivefold symmetry became more prominent. At T_g this process was slow and hysteresis was observed on heating [1]. Furthermore, it was found that the enthalpy curve for heating overshot and lay under the extrapolation of the equilibrium liquid curve [1]. When the heating and cooling curves finally met there was a maximum in the heat capacity, as is often observed for real glasses (see more details in [1]). On the other hand, Perchak and O'Reilly [2] presented the volume minimum of the SiO_2 system by cooling and heating again at the same cooling/heating rate using MD simulation. The volume-temperature curves showed hysteresis, i.e., the cooling and heating curves were different. This result was quite different from the MD simulation data in reference [3] using the same interatomic potential, where the cooling and heating curves were the same. This was explained by a longer holding time at each temperature, therefore the system in reference [3] was better equilibrated. However, the differences between structure and dynamics of models obtained at the same temperature by cooling and heating have not been investigated yet. Moreover, the existence of dynamic heterogeneities near the glass transition of atomic systems have been established [4–6]. Recently, dynamic heterogeneities in a more realistic atomic system of supercooled Al_2O_3 have been found [7] and maybe they are quite different in MOBC and MOBH. Therefore, our main aim here is the systematic analysis of the differences between structure and dynamics in such MOBC and MOBH of Al_2O_3 system through the study of PRDFs, coordination number distributions and dynamical heterogeneities.

2 Calculation

We carried out the MD simulations of Al_2O_3 models containing 3000 ions in a basic cube under periodic boundary conditions. The Born-Mayer type pair potential used here is of the form:

$$u_{ij}(r) = z_i z_j \frac{e^2}{r} + B_{ij} \exp\left(-\frac{r}{R_{ij}}\right) \qquad (1)$$

[a] e-mail: vvhoang2002@yahoo.com

where the terms represent Coulomb and repulsion energies, respectively. Here r denotes the distance between the centers of ith and jth ions; z_i and z_j are the charges of ith and jth ions; B_{ij} and R_{ij} are the parameters accounting for the repulsion of the ionic shells. Values $z_1 = +3$ and $z_2 = -2$ are the charges of Al^{3+} and O^{2-}. We have used the values $B_{11} = 0$, $B_{12} = 1779.86$ eV, $B_{22} = 1500$ eV and $R_{ij} = 29$ pm; details about the potentials and calculation method can be found in references [7–9]. Using such potentials we have successfully simulated structure and properties of liquid and amorphous Al_2O_3 [7–9]. The initial model at 7000 K has been obtained by heating the liquid Al_2O_3 model previously obtained in reference [8]. We then thermalized such model at 7000 K for 200 000 MD time steps to get an equilibrium initial configuration. We take this configuration as the starting point of a zero pressure run in which the temperature of the system was decreased linearly in time as $T(t) = T_0 - \gamma t$, where γ is the cooling rate, which is equal to 1.7178×10^{14} K/s, and T_0 is the initial temperature (=7000 K). This cooling process is continued until the system temperature is equal to zero. The so-obtained final configuration was subsequently relaxed at the zero temperature for 50 000 MD steps and was then heated up at zero pressure from 0 K to 7000 K with heating rate of 1.7178×10^{14} K/s. We have investigated MOBC and MOBH at three different temperatures of 2100 K, 3500 K and 5600 K. To calculate the coordination number distributions, we have used $R_{Al-Al} = 3.7$ Å, $R_{Al-O} = 2.2$ Å and $R_{O-O} = 3.3$ Å. Here R is a cutoff radius, which was chosen as the position of the minimum after the first peak in $g_{ij}(r)$.

3 Results and discussion

3.1 Enthalpy and density curves upon cooling and heating

Figures 1 and 2 present the temperature dependence of enthalpy and density of the Al_2O_3 system upon cooling and heating. Thermal hysteresis is clearly found only for the density of the system. At zero temperature, the density of the system is 2.67 g/cm^3 and is less than the smallest measured value of about 10%. However, the density of amorphous Al_2O_3 is not unique [10] and density of the system in the equilibrium state is not far from this one, measured in practice. It is essential to notice that the density of the Al_2O_3 system strongly increases with decreasing cooling rate [11] and we can reach the experimental value of density by a much lower cooling rate. It can be seen from Figure 2 that density of the system strongly increases upon cooling, while it slightly decreases upon heating in the temperature region of $T \leq 5000$ K. The deviation between the cooling and heating curves is enhanced with increasing temperature. This means that differences in structure and dynamics of the configurations obtained by cooling and heating at the same temperature can be expected and they are more pronounced with increasing temperature. This problem will be investigated and presented in the next subsections.

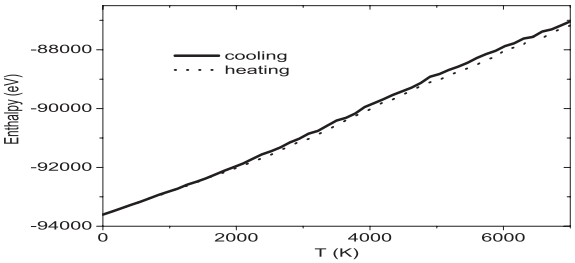

Fig. 1. Temperature dependence of the enthalpy of the Al_2O_3 system upon cooling and heating.

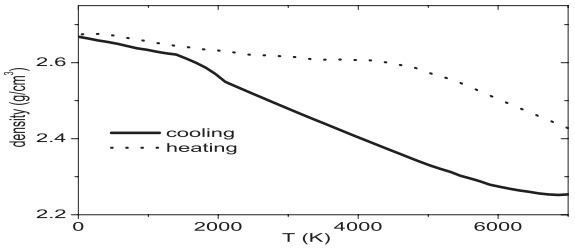

Fig. 2. Temperature dependence of the density of the Al_2O_3 system upon cooling and heating.

3.2 Static properties of the Al_2O_3 models at three different temperatures obtained by cooling and heating

In order to detect the differences in structure of Al_2O_3 MOBC and MOBH, we have saved the unrelaxed configurations at three different temperatures of 2100 K, 3500 K and 5600 K. The structure of unrelaxed models has been analyzed through PRDFs, coordination number distributions and interatomic distances.

Calculations show that the PRDFs of MOBC and MOBH at the temperature of 3500 K differ from each other by the height and position of peaks and differences are more pronounced for the Al–Al and O–O pairs (see Fig. 3). Similar results have been obtained for MOBC and MOBH at 2100 K and 5600 K (not shown). Table 1 shows that the height of the first peaks in PRDFs and mean coordination numbers for all atomic pairs of MOBH are larger than those of MOBC. In contrast, the differences in mean interatomic distances are not so large. As presented in [12,13] liquid Al_2O_3 has the structure of a tetrahedral network with the average coordination number $Z_{Al-O} \sim 4$. The structural element of the network is a slightly distorted $(AlO_4)^{5-}$ tetrahedron. The same structure also exists in our models (see Tab. 1). More details about the differences in structure of models can be found through coordination number distributions in MOBC and MOBH at the same temperature of 3500 K (see Fig. 4). Differences are more pronounced for the Al–Al and O–O pairs like those observed in MOBC and MOBH at the temperatures of 2100 K and 5600 K (not shown).

Figure 4 shows that although coordination number distributions for the Al–O pair of MOBC and MOBH are the same and they have a peak at $Z = 4$, indicating a similar tetrahedral network structure for both models, the differences can be found for the Al–Al and O–O pairs.

Table 1. Structural characteristics of unrelaxed Al_2O_3 models at three different temperatures obtained by cooling and heating. r_{ij} – Positions of the first peaks in the partial radial distribution functions (PRDFs) $g_{ij}(r)$; g_{ij} – The heights of the first peaks in PRDFs; Z_{ij} – The average coordination number (1–1 for the Al–Al pair, 1–2 for the Al–O pair, 2–1 for the O-Al pair, 2–2 for the O–O pair).

T (K)		r_{ij} (Å)			g_{ij}			Z_{ij}			
		1–1	1–2	2–2	1–1	1–2	2–2	1–1	1–2	2–1	2–2
2100	Cooling	3.24	1.75	2.83	2.71	5.93	2.20	7.51	4.13	2.75	7.80
	Heating	3.23	1.76	2.84	2.96	6.94	2.42	7.70	4.18	2.79	8.04
3500	Cooling	3.21	1.72	2.81	2.29	4.86	1.90	6.82	3.84	2.56	7.17
	Heating	3.20	1.76	2.81	2.73	5.82	2.21	7.40	3.90	2.60	7.66
5600	Cooling	3.21	1.70	2.80	2.16	4.56	1.81	6.15	3.45	2.30	6.41
	Heating	3.20	1.74	2.79	2.37	4.67	1.95	6.78	3.61	2.40	7.00
	*Exp.	3.25	1.78	2.84	1.70	5.60	2.40		4.20		

* Experimental data at 2473 K in [12,13].

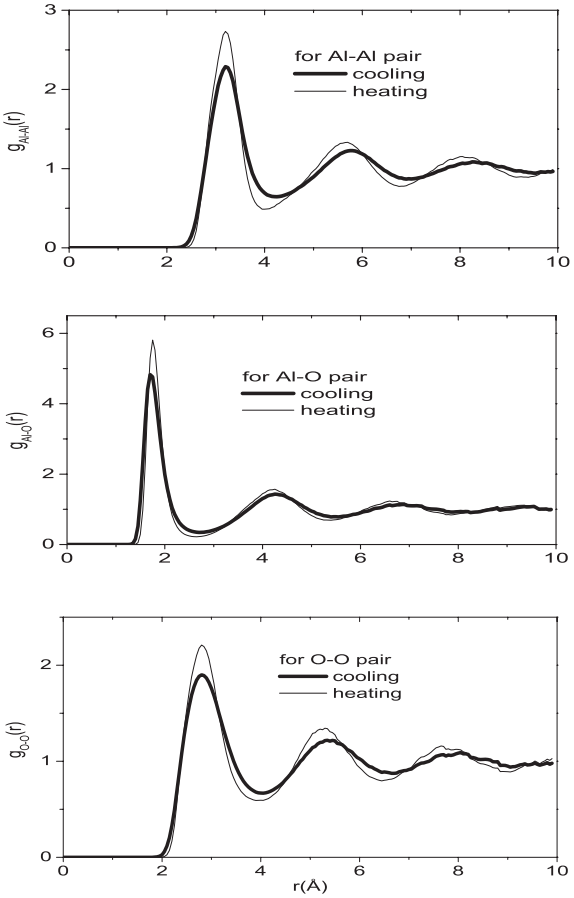

Fig. 3. Radial distribution functions in unrelaxed Al_2O_3 models at 3500 K obtained by cooling and heating.

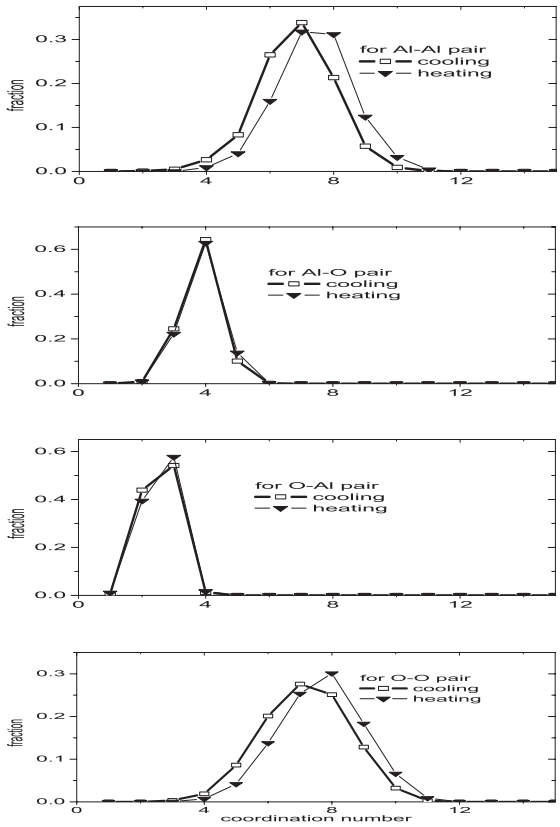

Fig. 4. Coordination number distributions in unrelaxed Al_2O_3 models at 3500 K obtained by cooling and heating.

This means that differences in the density of MOBC and MOBH lead to the different size of elementary structural units AlO_x and connectivity between them. It seems that such discrepancy will be enhanced in the high temperature region in accordance with the temperature dependence of density of the system (see Fig. 2 and Tab. 1). Detailed discussions of the bond-angle distributions in our Al_2O_3 system can be found elsewhere, for example in reference [7].

3.3 Dynamics of the Al_2O_3 models at 2100 K obtained by cooling and heating

In an effort to understand the strongly non-exponential relaxation behavior observed universally for liquids approaching the glass transition, much discussion over the past few years has focused on the question of dynamical heterogeneities [14]. Their presence has been uniquely shown by vastly different experiments [15–17]. Dynamical heterogeneities have also been observed by computer simulations [18–21] and many details about the relevance

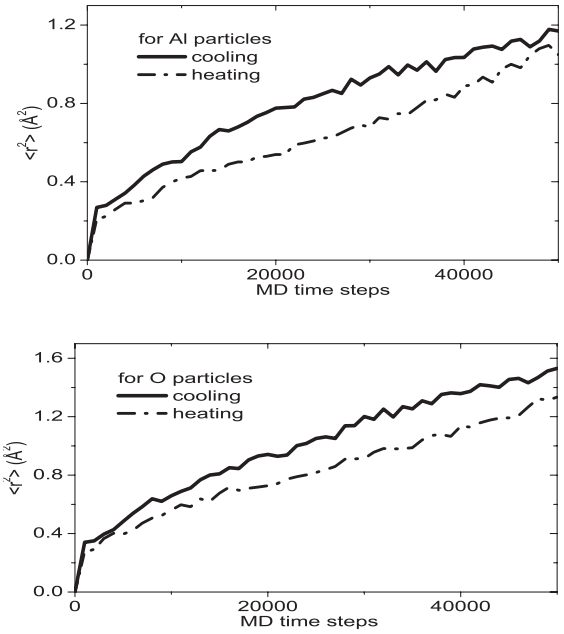

Fig. 5. Mean-squared atomic displacement distributions in Al_2O_3 models at 2100 K obtained by cooling and heating.

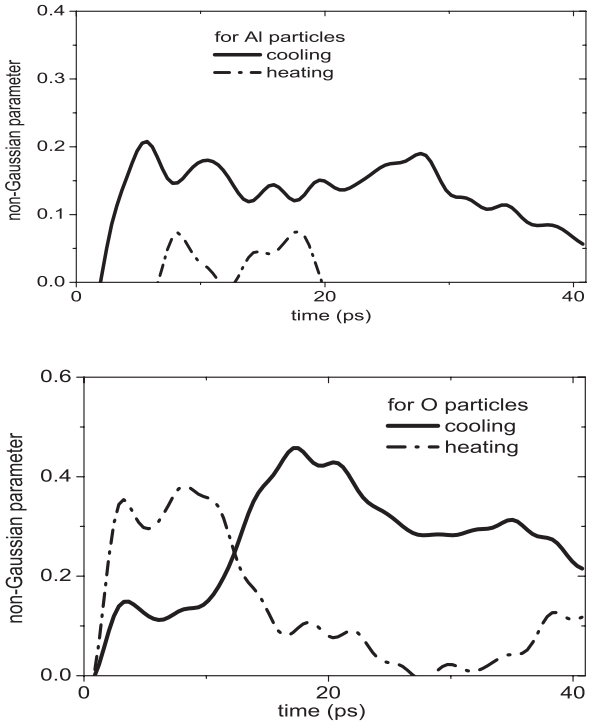

Fig. 6. Non-Gaussian parameter in Al_2O_3 models at 2100 K obtained by cooling and heating.

of dynamical heterogeneities, their time scale and length scale are therefore known today. It was shown that the length scale strongly increases with decreasing temperatures and the degree of cooperativity depends on the time scale with a maximum at a few times the α-relaxation time [22,23]. The dynamical heterogeneities in the simulated supercooled Al_2O_3 at 2100 K have been found and they strongly depended on the aging [7]. However, the nature of the dynamical heterogeneities have not been firmly determined and most previous work concentrated on the dynamical heterogeneities in the models obtained by cooling from the melt, with the exception of Lennard-Jones systems in reference [24], where Vollmayr-Lee et al. investigated the dynamical heterogeneities below the glass transition in a Lennard-Jones glass obtained by heating. On the other hand, the possibility of differences between dynamical heterogeneities in MOBC and MOBH has not been mentioned in reference [24] and such an interesting problem has not been investigated yet. Therefore, it is now studied in detail for our Al_2O_3 system.

First, one can see that the mean-squared atomic displacements of Al and O particles in MOBC and MOBH at 2100 K are quite different (Fig. 5). In the diffusion regime, the mean-squared atomic displacements of Al and O particles in MOBC are much larger than those in MOBH. The same phenomenon has been observed in MOBC and MOBH at 3500 K and 5600 K (not shown).

Second, dynamical heterogeneities in the system have been detected through the non-Gaussian parameter $\alpha(t)$ and the comparison of PRDFs of the 10% most mobile or immobile particles with the corresponding mean ones. The non-Gaussian parameter $\alpha(t)$ is of the form as follows (see more detail in Ref. [7]):

$$\alpha(t) = \frac{3\langle r^4(t)\rangle}{5\langle r^2(t)\rangle^2} - 1 \tag{2}$$

and is presented in Figure 6 are stronger than those in MOBH (see Fig. 6 and [25]).

Furthermore, we can also detect dynamical heterogeneities of the system by comparing the PRDF of the 10% most mobile or immobile particles with the corresponding mean ones. The deviation of PRDF for the 10% most mobile or immobile particles from the mean ones can be considered as evidence of dynamical heterogeneities [7,27] and this is also found in our Al_2O_3 system (see Figs. 7 and 8). The first peak in PRDF for the 10% most mobile or immobile Al particles is larger than for the mean, indicating the tendency of particles of extremely high or low mobility to be correlated. The mobile or immobile particles in MOBC are more strongly correlated than those in MOBH with the exception for the most immobile Al particles (see Fig. 8), however, the effect is not too strong.

We can estimate the tendency of the most mobile or immobile particles to form clusters in the model. To do this we have used the same rule as was done in reference [5], that is, two particles belong to the same cluster if their distance is less than the radius of the nearest neighbor shell. The radii of the nearest-neighbor shells are defined by the first minimum in PRDFs, $g_{ij}(r)$, and we have adopted the fixed values $R_{\mathrm{Al-Al}} = 3.7$ Å, $R_{\mathrm{Al-O}} = 2.2$ Å and $R_{\mathrm{O-O}} = 3.3$ Å, which were used for calculating the coordination number distributions. The probability

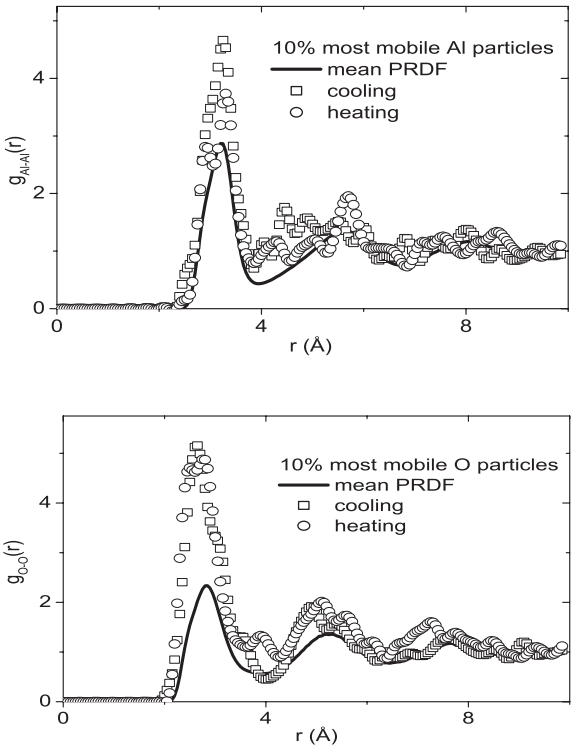

Fig. 7. Partial radial distribution functions for the Al–Al and O–O pairs in models at 2100 K obtained by cooling and heating; the solid line is for the mean particles in MOBC; the scatters are for the 10% most mobile Al and O particles.

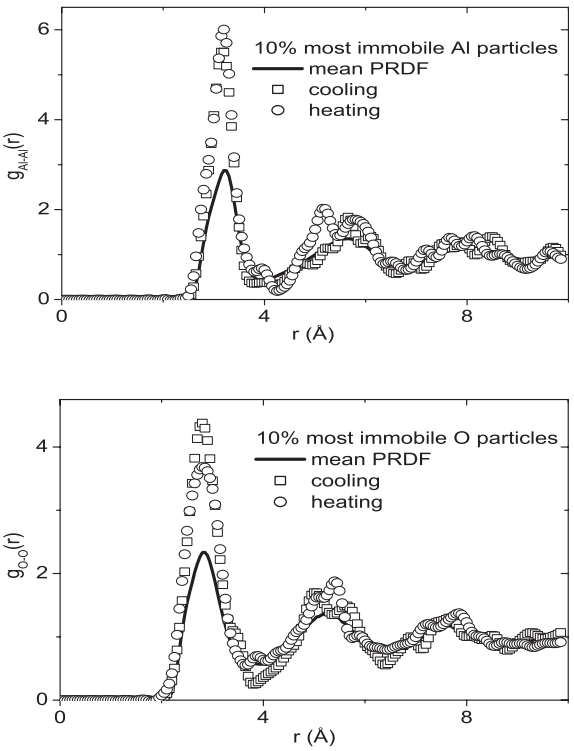

Fig. 8. Partial radial distribution functions for the Al–Al and O–O pairs in models at 2100 K obtained by cooling and heating; the solid line is for the mean particles in MOBC; the scatters are for the 10% most immobile Al and O particles.

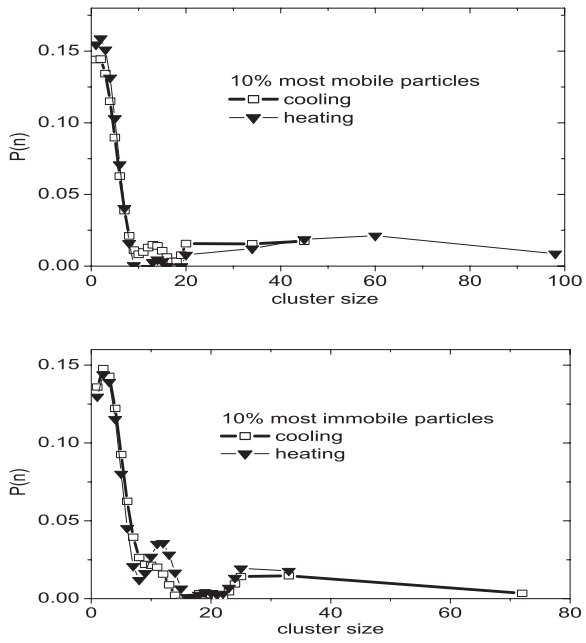

Fig. 9. Probability distribution of the size n of clusters of 10% most mobile or immobile particles in Al_2O_3 models at 2100 K obtained by cooling and heating.

distribution $P(n)$ of clusters of size n is shown in Figure 9, and we found a clear evidence of the tendency of most mobile or immobile particles to form clusters: they are not randomly distributed throughout the system. Here, we can find the significant differences in the probability distribution $P(n)$ of clusters of size n in MOBC and MOBH. Moreover, there is one largest cluster of most mobile particles containing 45 particles in MOBC contrary to 97 particles in MOBH. Meanwhile, for most immobile particles it contains 71 and 33 particles in MOBC and MOBH, respectively. It was found that as temperature decreases, the fraction of large clusters increases [26]. It can be suggested that the fraction of large clusters decreases with increasing temperature and is left for our consequent work in this direction concerning dynamical heterogeneities in the system obtained by heating.

4 Conclusion

We have investigated thermal hysteresis in the Al_2O_3 system obtained by cooling and heating. Our main conclusions are as follows:

(i) Indeed, thermal hysteresis exists in the Al_2O_3 system and is clearly found through the temperature dependence of density of the system upon cooling and heating.

(ii) Significant differences in static properties of Al_2O_3 models obtained by cooling and heating at three different temperatures of 2100 K, 3500 K and 5600 K have been found.

(iii) Significant differences in dynamic properties of Al_2O_3 models obtained by cooling and heating were also found. Moreover, the dynamical heterogeneities in Al_2O_3 models obtained by cooling and heating at the temperature of 2100 K are quite different.

References

1. H. Jonsson, H.C. Andersen , Phys. Rev. Lett. **60**, 2295 (1988)
2. D.R. Perchak, J.M. O'Reilly, J. Non-Cryst. Solids **176**, 211 (1994)
3. N. Kuzuu, H. Yoshie, Y. Tamai, C. Wang, J. Non-Cryst. Solids **349**, 319 (2004).
4. W. Kob, C. Donati, S.J. Plimpton, P.H. Poole, S.C. Glotzer, Phys. Rev. Lett. **79**, 2827 (1997)
5. C. Donati, S.C. Glotzer, P.H. Poole, W. Kob, S.J. Plimpton, Phys. Rev. E **60**, 3107 (1999)
6. A. Kerrache, V. Teboul, D. Guichaoua, A. Monteil, J. Non-Cryst. Solids **322**, 41 (2003)
7. V.V. Hoang, Shuk Kun Oh, Phys. Rev. E **70**, 061203 (2004)
8. V.V. Hoang, Phys. Rev. B **70**, 134204 (2004)
9. V.V. Hoang, Phys. Lett. A **335**, 439 (2005)
10. Because samples could contain a substantial amount of pores, and generally the density of amorphous alumina is not unique, i.e. ranging from 2.95 g/cm^3 to 3.30 g/cm^3
11. V.V. Hoang, to be published in Int. J. of Mod. Phys. B
12. C. Landron, A.K. Soper, T.E. Jenkins, G.N. Greaves, L. Hennet, J.P. Countures, J. Non-Cryst. Solids **293–295**, 453 (2001)
13. C. Landron, L. Hennet, T.E. Jenkins, G.N. Greaves, J.P. Coutures, A.K. Soper, Phys. Rev. Lett. **86**, 4839 (2001)
14. M.D. Ediger, C.A. Angell, S.R. Nagel, J. Phys. Chem. **100**, 13200 (1996)
15. K. Schmidt-Rohr, H.W. Spiess, Phys. Rev. Lett. **66**, 3020 (1991)
16. M. Yang, R. Richert, J. Chem. Phys. **115**, 2676 (2001)
17. M. Ediger, J. Chem. Phys. **103**, 752 (1995)
18. D.N. Perera, P. Harrowell, J. Chem. Phys. **104**, 2369 (1996)
19. R. Yamamoto, A. Onuki, Phys. Rev. E **58**, 3515 (1998)
20. S.C. Glotzer, J. Non-Cryst. Solids **274**, 342 (2000)
21. G.G. Malenkov, Physica A **314**, 477 (2002)
22. C. Bennemenn, C. Donati, J. Baschnagel, S.C. Glotzer, Nature **399**, 246 (1999)
23. B. Doliwa, A. Heuer, Phys. Rev. E **61**, 6898 (2000)
24. K. Vollmayr-Lee, W. Kob, K. Binder, A. Zippelius, J. Chem. Phys. **116**, 5158 (2002)
25. The curves of the non-Gaussian parameter of Al and O particles in supercooled Al_2O_3 model at the temperature of 2100 K differ slightly from those obtained in our previous article [26] due to different annealing before calculating the non-Gaussian parameter.
26. V.V. Hoang, S.K. Oh, J. Phys.: Condens. Matt. **17**, 5179 (2005)
27. It must be accounted for 5% particles detected from a tail of more mobile ones in the atomic displacement distribution. However, all results presented in the text are qualitatively the same if the 5% are replaced by 10%, but 10% include enough particles to obtain good statistics when examining their spatial correlation.